Numerical study on the effects of groundwater table oscillation beneath the "Palazzaccio" courthouse in Rome

Gorizia D'Alessio[1*], *Arianna* Pucci[1], *Giulia* Guida[1] and *Francesca* Casini[1]

[1] University of Rome 'Tor Vergata', Department of Civil Engineering and Computer Science, 00133 via del Politecnico 1, Rome

Abstract. This work aims to evaluate the settlement induced by the river Tiber groundwater table oscillations. A representative section of the subsoil beneath the courthouse "Palazzaccio", close to the river in the city centre of Rome, is analysed via the finite element method with a fully coupled hydro-mechanical model. The effects of wetting-drying cycles induced by the water table oscillation are accounted for by adopting the Barcelona Basic Model for the unsaturated layers, whose model parameters are calibrated using experimental results on saturated and unsaturated samples and literature data. The variation of the river Tiber level is reconstructed according to the *"Tevere – Ripetta"* hydrometric station records between 2005 and 2008, and it is applied as a boundary condition at the boundary of the model domain.

1 Introduction

The damage to monuments and historic buildings in the historic centre of Rome could be related to the fluctuation in the superficial water table connected to the Tiber hydraulic regime [1-3]. The seasonal variation of the Tiber flow and, thus, of its hydraulic level results in a seasonal oscillation of the depth of the water table. The superficial subsoil layers, constituted by made ground, are subjected to drying and wetting cycles which may lead to an accumulation of displacements, mainly when saturation collapse occurs [4-6]. This sudden and irreversible phenomenon is typical of loose and heterogenous soils [7] during the imbibition process. The made ground layers of the historic central areas of Rome adjacent to the Tiber are generally characterised by loose and heterogeneous sandy-silty soils.
In the future, due to the expected progressively extreme events related to climate changes, the river would exacerbate its hydraulic regimes, with massive flood waves alternating with periods of lean [8].

2 Case study

The analysed geotechnical section is located on the west bank of the Tiber River, between the Tiber Embankment (*Lungotevere*) and the Cavour Square, beneath the Palace of Justice (also known as 'Palazzaccio'). The latter was built between 1889 and 1911 and represents one of the significant monumental works carried out after the proclamation of Rome as the capital of the Kingdom of Italy. Currently, it hosts the Supreme Court of Justice and the Council of the Lawyers Association of Rome. The building has a regular plan, with dimensions of 170 m per 154 m. It comprises three bodies, a central taller building (40 m high) and two buildings at the sides (26 m high). Due to the varying height and the variety of heavy materials used during its construction (rock blocks and brick masonry), the loads at the foundation plane are high and not uniformly distributed [1]. The foundation slab, approximately 2 m thick, is founded at 9 m depth from the surface in the made ground layer. The building suffered structural problems and damages from the beginning due to differential soil settlements [1]. A technical committee was set up in 1970 to investigate the causes and solutions to the soil settlements problem. The analysis of the evolution of the displacement with time revealed a greater displacement rate of the points of the building closer to the river Tiber (at about 60 m). However, the subsoil layers on the opposite side of Cavour Square are more deformable. Thus, the cause of the differential settlements was attributed to the fluctuations in the shallow GWT level [1].

2.1 Stratigraphy

Fig.1 shows the stratigraphy profile under the "Palazzaccio" reconstructed from the available data and geognostic surveys [1,9-12]. The subsoil is divided into six different lithotypes (from the top): a made ground layer (MG) of almost constant thickness equal to 10 m, characterised by loose and heterogeneous sandy-silty soils; a clay silt layer (CS) highly compressible and poorly permeable, with variable thickness between 3 m and 7 m; a fine sand layer (FS), moderately permeable, with a thickness of 5 m that increases toward the Tiber river; a clay organic silt layer (OS) which is characterised by high compressibility and low permeability, with thickness until a maximum of 20 m. Finally, 6 m of fine sand and a gravel layer follow. The average level of the shallow GWT lies between the MG

* Corresponding author: gorizia.d.alessio@uniroma2.it

and the CS layers, and its regime is supposed to be correlated to the river Tiber level.

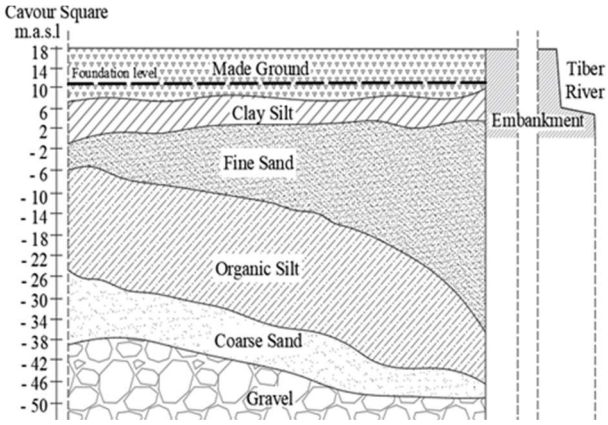

Fig.1: Stratigraphy profile beneath "Palazzaccio" [1]

2.2 Hydraulic Regime

The records of the hydrometric station "*Tevere – Ripetta*", located beneath the bridge of *Cavour*, are retrieved by hydrological annals available on the website of the *Regione Lazio* (http://www.idrografico.regione.lazio.it/). Fig.2 shows the evolution of the hydrometric level of the Tiber River between the years 2005 and 2008 considered in the study. Several floods are identified: F1 is February 2005, F2 November 2005 and F3 November 2008.

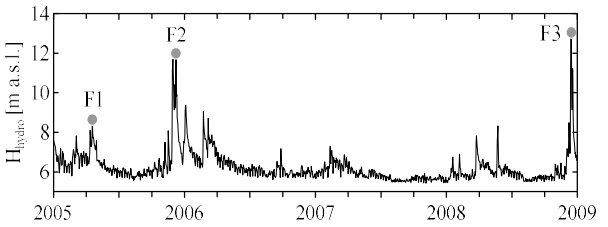

Fig.2: Evolution of the Hydrometric Heights of the Tiber river among the years 2005 – 2008: *Tevere – Ripetta* Hydrometric Station

3 Numerical modelling

The fully coupled hydro-mechanical analyses are performed with COMSOL Multiphysics®, adopting a two-dimensional stratified geometry (Fig. 5). The depth of the bedrock is assumed at 52 m from the ground surface. Depending on the seasonal oscillations, the groundwater table depth is located between the made ground layer and the silty soil layer. The BBM (Barcelona Basic Model) [13] was adopted for these two layers, while the deeper layers are assumed to be linear elastic.

3.1 Balance equations

The governing equations used to solve the hydro-mechanical problem were the equilibrium equation (Eq.1) and the water mass balance equation (Eq. 2). The airflow was neglected.

$$\nabla \cdot \boldsymbol{\sigma} + \boldsymbol{f} = 0 \tag{1}$$

$$d(n \cdot S_r \cdot \rho_w)/dt + \nabla \cdot (\rho_w \boldsymbol{v}) = 0 \tag{2}$$

where σ is the stress tensor, $\boldsymbol{f}$ is the vector of external forces, n is the porosity, S_r is the degree of saturation, ρ_w is the density of water, and $\boldsymbol{v}$ is the velocity field of liquid water described by Darcy's law (Eq.3):

$$\boldsymbol{v} = - \boldsymbol{K}_{sat}\, k_{rel}(S_r)\, \nabla \cdot (z + \boldsymbol{p_w}/\gamma_w) \tag{3}$$

where $\boldsymbol{K}_{sat}$ is the hydraulic conductivity tensor**,** k_{rel} is the relative permeability, defined in Section 3.3 as a function of S_r, z is the elevation, and p_w is the pore water pressure. The independent variables for the problem are the field of displacement u (Eq.1) and the pore water pressure p_w (Eqs.2-3), respectively, for the mechanical and hydraulic parts. Further, the water retention curve (WRC) describing S_r as a function of p_w fully couples the three equations.

3.2 Calibration of BBM parameters

The BBM was adopted for unsaturated layers (MG and CS). The BBM parameters were calibrated from experimental data. Three oedometer tests (Fig. 3a) were carried out on unsaturated silty sand specimens extracted from the MG layer. The three tests are distinguished by the initial conditions (void ratio, natural water content) and the vertical net stress at which the saturation phase was applied: T1 started from $e_{initial}$=1.40, $w_{initial}$=38%, $S_{r,initial}$=73% and the saturation phase occurred at 50 kPa, T2 started from $e_{initial}$=1.25, $w_{initial}$ =38%, $S_{r,initial}$ =82% and the saturation at 100kPa, and finally, T3 started from $e_{initial}$=1.27, $w_{initial}$ =38%, $S_{r,initial}$=81% and the saturation at 200 kPa. Indeed, the samples began the compression loading in unsaturated conditions. They were progressively saturated at an intermediated vertical net stress, and finally, they completed the compression load in fully saturated conditions.

The BBM parameters of the CS layer are calibrated on the experimental data reported by [16] on silt specimens with initial void ratio $e_{initial}$=0.86 and $e_{initial}$=0.81, initial water content $w_{initial}$=13%, and initial degree of saturation $S_{r,initial} \approx 40\%$.

Fig. 3 shows the comparison between the model predictions and the experimental data from the oedometer tests carried out on the MG (Fig.3a) and CS specimens (Fig.3b). The parameters adopted are summarised in Tab.1.

For MG specimens (Fig.3a), the model predictions are satisfactory for both the initial compression phase in unsaturated conditions and the saturation phase at constant vertical stress. In contrast, the model slightly underestimates the slope of the normal compression line in fully saturated conditions. For CS specimens (Fig. 3b), the model adequately predicts the slope of NCL in unsaturated conditions and slightly underestimates the variation in void ratio due to saturation collapse, with an average difference of about 2%.

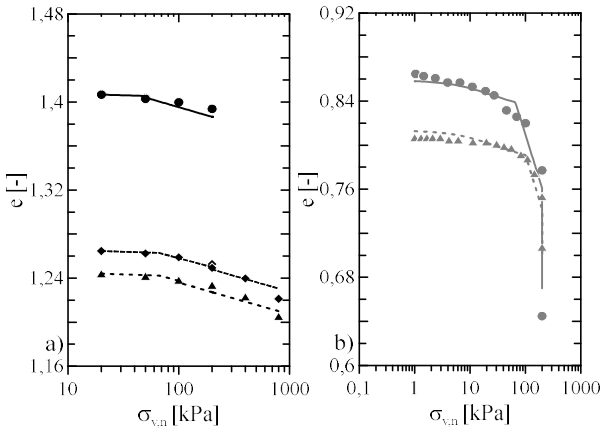

Fig.3 : Comparison between numerical results and experimental data: a) MG B) CS

Tab.1: BBM parameters.

	MG	CS
λ_0	0.013	0.08
λ_s	0.015	0.002
r	0.300	0.550
β	0.015 kPa^{-1}	0.025 kPa^{-1}
κ	0.0019	0.005
κ_s	0.002	0.0012
p_c	25 kPa	4.8 kPa

The parameters obtained from the calibration show a lower compressibility of the MG samples under fully saturated conditions ($\lambda_{0,MG} < \lambda_{0,CS}$) and a lower rate of change in stiffness under variation of suction ($\beta_{MG}<\beta_{CS}$).

Table 2 shows the initial and physical parameters of the MG and CS layers used to perform the numerical analyses: the unit weight γ, pre-consolidation stress for saturated condition p_0^* and initial void ratio *e*.

Table 3 summarises the physical and constitutive parameters used for the linear elastic layers (FS and OS), chosen from literature data [9 - 12]: the unit weight γ, the Young modulus *E* and the Poisson ratio ν.

Tab.2: Physical and initial parameters for the unsaturated layers adopted for the numerical analyses.

	MG	CS
γ	19 kN/m^3	17 kN/m^3
p_0^*	55 kPa	40 kPa
$e_{initial}$	1.30	0.85

Tab.3: Physical and constitutive parameters for the linear elastic layers adopted for the numerical analyses.

	FS	OS
γ	20 kN/m^3	17.50 kN/m^3
E	60 MPa	20 MPa
ν	0.30	0.30

3.3 Water Retention Curve Model

The water retention curve (Eq.5) and the relative permeability function (Eq.6) were defined by the van Genuchten models [14].

$$S_r = S_{res} + (1-S_{res}) \cdot [(1+s/P)^n]^{-m} \quad (5)$$

$$k_{rel}(S_r) = S_e^{0.5} \cdot [1-(1-S_e^{1/m})]^2 \quad (6)$$

where S_{res} is the residual degree of saturation, *s* is the suction, *P* is the air entry value, *m, n* are the model parameters, and S_e is the effective saturation ($S_e = (S_r - S_{res})/(1-S_{res})$).

The WRC parameters were calibrated from the grain size distribution and the initial porosity by the Arya & Paris method [15]. The Jossigny silt WRC is adopted from [16]. Fig. 4 shows the water retention curves adopted for MG and CS layers. The parameters adopted are summarised in Tab 4.

Tab.4: Hydraulics parameters for the unsaturated layers

	MG	CS
$S_{r,res}$	0.20	0.25
P	20 kPa	13 kPa
m	0.63	0.67
n	2.686	3.03

The saturated hydraulic conductivities adopted from the literature [12] are the following: K_{sat} = 5e-5 m/s for the made ground layer, K_{sat} = 5e-6 m/s for the clay silty one, K_{sat} = 5e-4 m/s for the silty-fine sand and K_{sat} = *5e-7* m/s for the clayey organic silt.

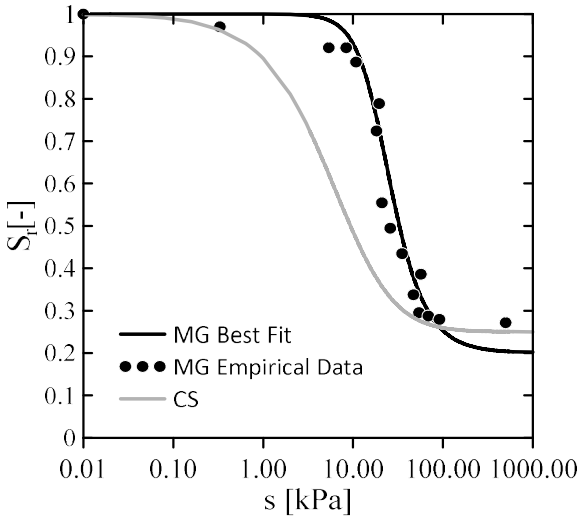

Fig. 4: WRC for MG (black line) and CS (grey line) layers [9]

3.4 ICs and BCs

The simulations started from an undeformed condition with a pore water pressure profile due to the GWT's initial position, located at 7.45 m a.s.l, corresponding to 10.55 m depth from ground level. To replicate the lithostatic conditions due to gravity loading, a steady-state phase was first carried out, in which gravity was

applied. The Tiber river was taken into account by imposing boundary conditions on the right edge of the domain in terms of the water pressure depending on time, according to the hydrometric level of the river (Fig. 2). While on the opposite edge, a no flux condition was applied. Sliders and hinges were applied on both sides and at the base, respectively. Fig. 5 shows the schematic domain with a summary of the boundary conditions imposed and the initial position of the GWT.

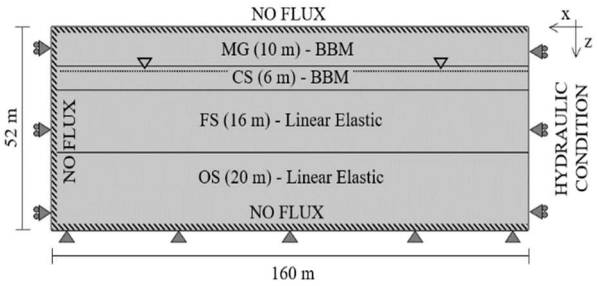

Fig.5: Geometry domain and boundary conditions

4 Results

Fig.6a shows the evolution of the total displacements over time for the MG (black lines) and the CS layers (grey line) at two different distances from the river: x=10 m (dashed lines) and x=60 m (continuous lines) and the evolution of hydrometric heights. After F1 and F2 flood, in February and November 2005, respectively, a significant accumulation of displacements occurred in both layers due to saturation collapse, with more emphasis on the MG layer. The latter is due to the MG layer's more significant pore water pressure variations during groundwater oscillations. Fig. 6b reports a zoom on the evolution of the displacements of the MG layer during the F2 flood event (27-30 November 2005). While at x=10 m from the river, the increase of displacements in the MG layer occurred simultaneously with the river level rising; at x=60 m, they happened with a delay of about four days. In addition, after the flood of November 2005 (F2), the displacements of the MG and the CS layers are 11 mm and 1 mm, respectively, at a distance of x=10 m from the river, while they decrease to 9 mm and almost ~0 mm respectively at a distance x=60 m from the river.

Fig. 7 shows the evolution of volumetric plastic strain with time for the MG and CS layers, together with the hydrometric river heights. Volumetric plastic strains occurred in the unsaturated layers after flood events. Interestingly, although flood F3 was more significant in intensity than flood F2, it produced less volumetric plastic strain. During the F3 flood, an initial elastic swelling was predicted, followed by saturation collapse. The initial elastic swelling was due to the increased preconsolidation pressure, led by past saturation collapse events.

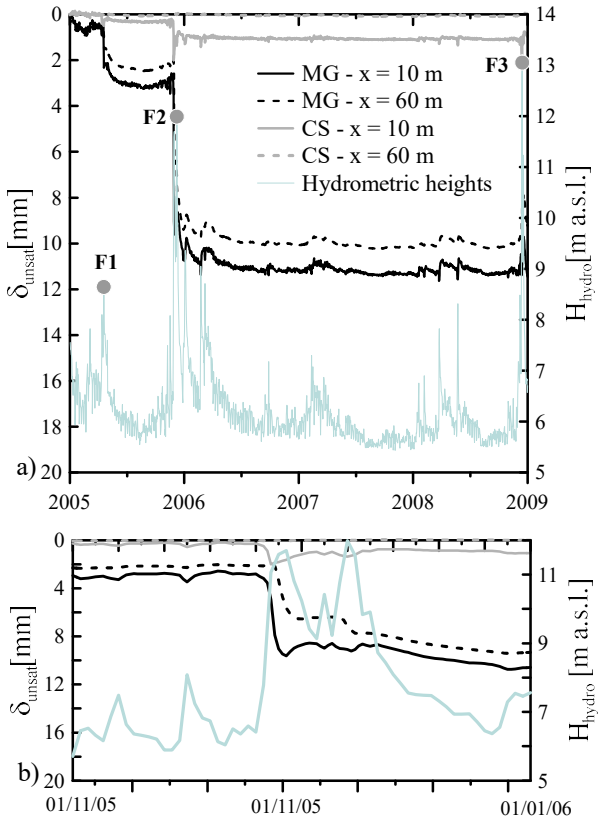

Fig.6: a) Evolution with time of displacements and hydrometric heights of the river Tiber b) Zoom of the displacement around the F2 flood event.

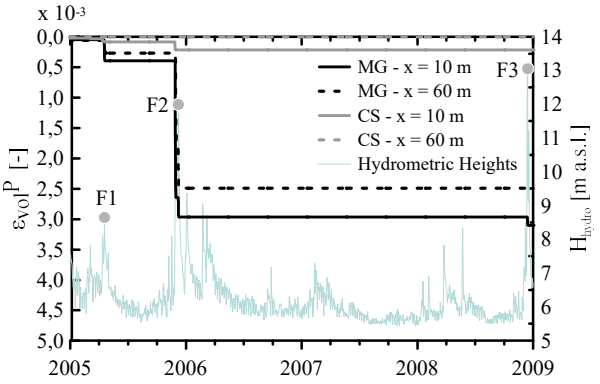

Fig.7: Volumetric plastic strain and hydrometric heights over time

Fig 8 reports the profiles of volumetric plastic strain and pore water pressure over depth for the unsaturated layers, at the distance of (a) x=10 m and (b) x=60 m from the river, for the three flooding events, F1, F2, and F3. A greater susceptibility to saturation collapse was experienced by the MG layer between depths from 4 m to 10 m. Increasing the distance from the river, the CS layer reduced the maximum plastic strain accumulated after the three flood events from 0.04% to ~0%. The plastic deformations decreased from 0.3% to 0.25% in the MG layer. The depth of the maximum volumetric plastic strain was related to the height of the GWL achieved during the flood event, which increased from F1 to F3.

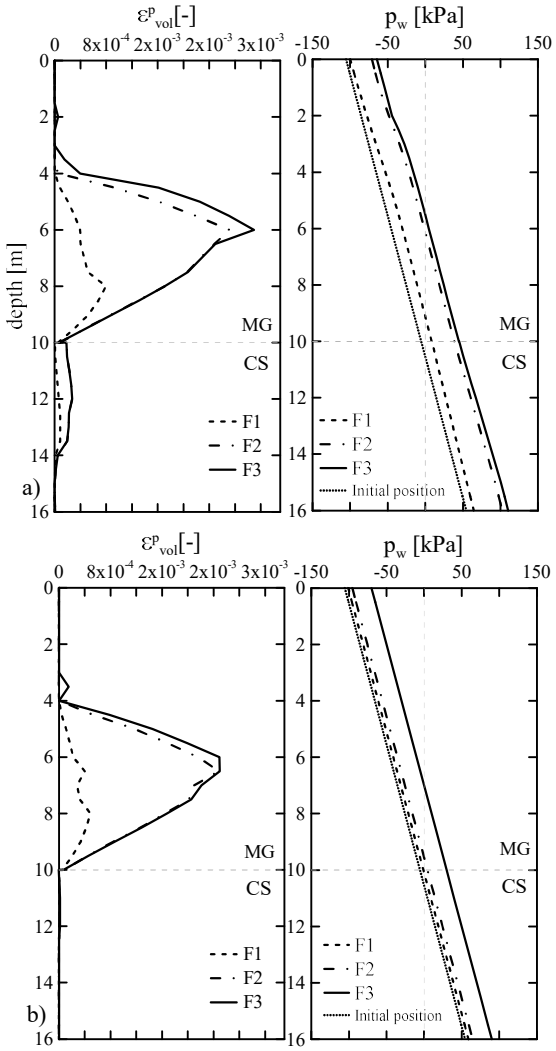

Fig.8: Profile of volumetric plastic strains and pore water pressure over depth: a) 10 m b) 60 m

5 Conclusions

This study numerically simulated the soil deposit response beneath the Rome courthouse "Palazzaccio" due to the groundwater table oscillations using the unsaturated soil framework. The study uses a two-dimensional finite element model that accurately reproduces the Tiber River hydraulic regime.

The displacement accumulated with time (2005-2008) showed a strong connection with the GWT variations: after the first flood F1, the displacement increased to 3 mm, and after the second flood F2, up to 11 mm. In contrast, the most severe flood F3 did not produce further significant displacement due to the yielding of the past events that led to an increase in the pre-consolidation pressure. The made ground layer exhibits greater displacements due to the significant increases in the pore water pressure.

This work is part of Tiber'S research project that aims to monitor and assess the effects of groundwater fluctuations by monitoring the satellite data displacement. The data predicted well agreed in magnitude with the satellite data of the area.

The financial support of LazioInnova through the project 'Tiber's' is acknowledged (project number A0375-2020-36632, 22/07/2021). The first and second author acknowledges MUR for support of their fellowships through the DM 351 (09/04/2022) PNRR – M4C1 – Inv. 4.1 and PON/DM 1061 (10/08/2021), respectively.

References

1. M. Amanti, G. Gisotti, M. Pecci, *I dissesti a Roma - Memorie descrittive della Carta Geologica d'Italia,* Vol. 50, 219 – 248, ISBN: 978-88-240-3970-3, Rome (1995)
2. I. Giannetti, Casini F., *The construction and the collapse of the Tiber retaining walls in Rome, Italy (1870 – 1900),* Proceeding of the Institution of Civil Engineers – Engineering History and Heritage, Vol. 152, 48 – 58, (2022)
3. Casini F., Pucci A., Giannetti I., Guida G., *Geotechnical and historical aspects on the collapse of the Tiber embankment walls in the centre of Roma (1870 – 1900)*, Geotechnical Engineering for the Preservation of Monuments and Historic Sites III, CRC Press, 1206-1214, (2022)
4. A. Gens, *Soil – environment interactions in geotechnical engineering,* Gèotechnique 60, No. 1, 3 – 74, (2010)
5. Casini F., *Deformation induced by wetting: a simple model,* C Canadian Geotechnical Journal, 49: 954–960 (2012)
6. Rotisciani, G.M., Lalicata, L.M., Desideri, A., Casini, F., *Numerical modelling of the response of an unsaturated silty soil under wetting and gravitational loading processes*, In 4th European Conference on Unsaturated Soils, E-UNSAT (2020)
7. Vilar O.M., Rodrigues R.A, *Collapse behavior of soil in a Brazilian region affected by a rising water table*, Canadian Geotechnical Journal, 48(2): 226 – 233 (2011)
8. Pucci A., D'Alessio G., Giannetti I., Moriero I., Guida G., Guerrero Tello J.F., Moccia B., Russo F., Marsella M., Casini F., *Geotechnical alanyses on the effects of Tiber River Hydraulic regime in the city centre of Rome within the project Tiber'S,* In VIII Convegno Nazionale dei Ricercatori di Ingegneria Geotecnica – CNRIG (2023)
9. U. Ventriglia, La geologia della città di Roma, Amministrazione Provinciale di Roma, (1971)
10. U. Ventriglia, *Idrogeologia della Provincia di Roma,* Amministrazione Provinciale di Roma, (2002)
11. A. Corazza, M. Lanzini, C. Rosa, R. Salucci, *Caratteri stratigrafici, idrogeologici e geotecnici delle alluvioni tiberine nel settore del centro storico di Roma,* Italian Journal of Quartenary Sciences, n. 12, 215 – 235, (1999)
12. C. Di Salvo, M. Mancini, M. Moscatelli, M. Simionato, G.P. Cavinato, M. Dimasi, F. Stigliano, *From Lithological Modelling to Groundwater*

Modelling: A case study in the Tiber River Alluvial Valley, Geosciences, 11, 507, (2021)

13. Alonso, E. E., Gens, A., Josa, *A., A constitutive model for partially saturated soils*, Géotechnique, 40(3), 405-430 (1990)
14. Van Genuchten, M. T., *A closed-form equation for predicting the hydraulic conductivity of unsaturated soils*, Soil science society of America journal, 44(5), 892-898 (1980).
15. Arya, L. M., Paris, J. F., *A physicoempirical model to predict the soil moisture characteristic from particle-size distribution and bulk density data*, Soil Science Society of America Journal, 45(6), 1023-1030 (1981)
16. Casini F., *Effetti del grado di saturazione sul comportamento meccanico di un limo,* PhD Thesis, University of Rome "La Sapienza", Italy (2008)